Calculation of melt pond albedos on arctic sea ice

ALEXANDER P. MAKSHTAS and IGOR A. PODGORNY

An analytical approximation of spectral albedo is derived for a melt pond with a Lambertian bottom assuming that Rayleigh scattering in the water is small compared to absorption. A Monte Carlo method is used to verify that scattering can be ignored in the water. This enables us to calculate pond albedos in the 400–700 nm wavelength band using the analytical approximation. Model calculations and observations indicate that a step-decrease in albedo is likely to occur when a melt pond initially forms, and melt pond albedos in the visible depend more on the structural and optical properties of the bottom than on the depth of the pond.

A. P. Makshtas, Arctic & Antarctic Research Institute, 38 Bering st., 199397, St. Petersburg, Russia; I. A. Podgorny, University of Washington, JISAO, P.O. Box 354235, Seattle, WA 98195, USA

Introduction

Melt ponds represent an important component of the arctic climate system. They greatly affect both the surface albedo and redistribution of solar energy in the sea ice cover during the melt season (e.g. Maykut 1986; Maykut & Perovich 1987; Barry et al. 1993; Ebert & Curry 1993; Ebert et al. 1995).

Over the past few decades a large quantity of albedo measurements have been reported for melt ponds (e.g. Nazincev 1964; Langleben 1971; Grenfell & Maykut 1977; Grenfell & Perovich 1984; Ivanov & Alexandrov 1994; Perovich 1994; Morassutti & LeDrew 1995). The measurements span the entire season and include observations for a variety of ice types and illumination conditions. For example, according to Nazincev's (1964) observations in the central part of the Arctic basin, melt ponds having an albedo as low as 0.3 covered up to 45% of the surface. As a result, area-averages albedos of the surface were as low as 0.45 in July. In addition to empirical studies, the effect of melt ponds on the short-wave radiative transfer has been studied using a coupled atmosphere-ocean-sea ice model (Jin et al. 1994).

Despite this considerable effort, there is a need for better knowledge of how solar energy is redistributed in the ponded ice (Moritz et al. 1993). While there do exist some empirically obtained parameterisations for melt pond albedos and radiative fluxes into the melt water layer (Ebert & Curry 1993; Ebert et al. 1995; Morassutti & LeDrew 1995), a theoretical basis for these parameterisations is still absent. As outlined by Moritz et al. (1993), spectral albedo models for melt ponds must be formulated taking into account ice thickness, melt pond area and thickness, lead fraction, ice age, salinity and snow characteristics. Investigation of how melt pond albedo is affected by each of these parameters will yield an improved understanding of the relationship between summer albedos and melt processes. This paper presents new data on pond albedos in the Arctic Ocean in the 400–700 nm band and describes a method for calculating spectral albedos of melt ponds. Only the visible spectrum is considered because pond albedos in the solar infrared are determined primarily by Fresnel reflection and are nearly independent of wavelength (e.g. Grenfell & Maykut 1977). Both measured and calculated albedos are analysed as a function of pond depth.

We do not attempt to present a definitive parameterisation of pond albedo that could be incorporated into the sea-ice models. Instead, the objectives of this paper are twofold: (1) to increase the understanding of the short-wave radiative transfer in melt ponds and (2) to develop a forward model that can be applied in estimating

the vertical partitioning of solar energy in a melt pond and underlying ice from measurements of pond albedo and depth.

Spectral albedo of melt ponds

Statement of the problem

Because many details of the inherent optical properties of ponded ice are still uncertain, *a priori* prescribed spectral albedos of the melt pond bottom are used in numerical simulations of radiative transfer within the ice layer. The ice is assumed to be optically thick, while the reflectance distribution of the pond bottom is assumed to be Lambertian and independent of the angular distribution of the incident radiance. Optical properties of the melt water are postulated to be similar to the optical properties of the clearest water observed in the central part of the Arctic Basin (Smith 1973).

The configuration of the model used in this study is shown in Fig. 1. The model consists of two plane-parallel layers, hereafter referred to as the water and ice layers. Both layers are assumed to be optically homogeneous in the vertical and horizontal directions. Spectral albedo (α) is denoted by the subscript w for the water in the melt pond itself and by the subscript i for the ice at the pond bottom. Melt pond depth is denoted by h_w.

The directions defining the incoming and outcoming light beams in the atmosphere are expressed by (μ, ϕ), where μ is the cosine of the zenith angle and ϕ is the azimuthal angle. Furthermore, μ and $-\mu$ denote upward and downward directions. The direction of the incoming solar beam is denoted by $(-\mu_0, \phi_0)$. Similarly, the direc-

tions defining the light beams in the water layer are expressed by (η, ϕ), with η and $-\eta$ denoting upward and downward directions respectively. The direct solar radiation reaching the air-water interface from above (F_0) is refracted into the direction $(-\eta_0, \phi_0)$ in accordance with Snell's law

$$\sqrt{1 - \mu_0^2} = n_w \sqrt{1 - \eta_0^2}, \qquad (1)$$

where n_w is the refractive index of the water. The n_w value is taken to be 1.33 in this study, irrespective of wavelength.

We start by considering the monochromatic radiative transfer equation in one spatial dimension for the water layer. Specifically,

$$\eta \frac{dI(\tau, \eta, \phi)}{d\tau} = I(\tau, \eta, \phi)$$
$$- \frac{\Lambda_w}{4\pi} \int_0^{2\pi} d\phi' \int_{-1}^1 I(\tau, \eta', \phi') x(\gamma) d\eta'$$
$$- \frac{(1 - R(\mu_0))\Lambda_w x(\gamma')F_0 \exp\left(-\dfrac{\tau}{\eta_0}\right)}{4\pi}, \qquad (2)$$

where γ and γ' are determined by

$$\cos(\gamma) = \eta\eta' \qquad (3)$$
$$+ \sqrt{(1 - \eta^2)(1 - \eta'^2)} \cos(\phi - \phi')$$

$$\cos(\gamma') = \eta\eta_0 \qquad (4)$$
$$+ \sqrt{(1 - \eta^2)(1 - \eta_0^2)} \cos(\phi - \phi_0).$$

Here, $I(\tau, \eta, \phi)$ is the unpolarised diffuse spectral radiance at wavelength λ (omitted for brevity) at optical depth τ, Λ_w is the single-scattering albedo, $x(\gamma)$ is the phase function, γ is the scattering angle ($0 \leqslant \gamma \leqslant 180°$), $R(\mu_0)$ denotes the Fresnel reflection coefficient for the air-water boundary, and F_0 is the incident spectral irradiance. As seen from Fig. 1, optical depth increases with the depth of the water layer.

In addition to Eq. (2), which governs the transfer of diffuse radiation, we introduce the transfer equation for direct radiation in the water layer:

$$F_{dir}^{\downarrow}(\tau) = (1 - R(\mu_0))F_0 \exp\left(-\frac{\tau}{\eta_0}\right). \qquad (5)$$

The direct component of the radiation field is associated with that part of the unscattered solar flux which penetrates through the air-water interface and is attenuated exponentially.

The boundary condition at the top of the water layer is given by

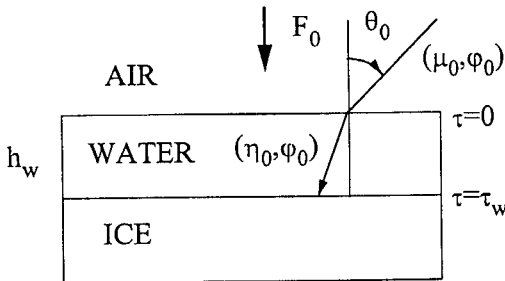$$I^{\downarrow}(0, -\eta, \phi) = R(\eta)I^{\uparrow}(0, \eta, \phi), \qquad (6)$$

Fig. 1. Configuration of the one-dimensional melt-pond model.

while downwelling radiation at the top of the ice layer is

$$\pi I^{\downarrow}\,(\tau_w) = \alpha_i \int_0^{2\pi} d\phi' \int_0^1 d\eta' I^{\downarrow}\,(\tau_w, -\eta', \phi')\,\eta' + \alpha_i\, F_{dir}^{\downarrow}\,(\tau_w). \tag{7}$$

Here, $\tau_w = (\kappa_w + \sigma_w)|h_w|$ is the optical thickness of the water layer, κ_w and σ_w are the beam absorption and scattering coefficients in the water, and $R(\eta)$ is the Fresnel reflection coefficient for the water-air interface. Eq. (6) describes the Fresnel reflection of the upwelling diffuse radiation from the top surface of the water layer. Eq. (7) describes the diffuse reflection of the downwelling direct and diffuse radiation from the top surface of the ice layer. $I^{\uparrow}$ and $I^{\downarrow}$ denote the upwelling and downwelling radiances respectively. Because the pond bottom is assumed to be a Lambertian reflector, η and ϕ are omitted in the left side of Eq. (7).

The problem is formulated as follows: Under the assumption that scattering is small compared to absorption, one needs to find an approximate (analytical) solution to Eq. (2) with the boundary conditions given by Eqs. (6) and (7). The accuracy of the analytical solution must then be estimated for actual τ_w and Λ_w values.

Analytic solution to the radiative transfer equation

When scattering in the water layer is small compared to absorption, the diffuse radiation field is independent of the azimuthal angle for any η and τ because the only source of diffuse radiation in this case is the reflection from the melt pond bottom in accordance with Eq. (7). Inserting a delta-function for the phase function into the right side of Eq. (2), integrating over η' and ϕ' and dividing by $(1 - \Lambda_w)$, we reduce the transfer equation for the diffuse radiation to the differential form of Beer's law:

$$\eta\frac{dI(\tilde{\tau}, \eta)}{d\tilde{\tau}} = I(\tilde{\tau}, \eta), \tag{8}$$

where

$$\tilde{\tau} = (1 - \Lambda_w)\tau. \tag{9}$$

In terms of $\tilde{\tau}$, boundary condition (7) is expressed as

$$\pi I^{\uparrow}\,(\tilde{\tau}_w) = \alpha_i \left(2\pi \int_0^1 I^{\downarrow}\,(\tilde{\tau}_w, \eta')\eta' d\eta' + F_{dir}^{\downarrow}\,(\tilde{\tau}_w) \right), \tag{10}$$

where the optical thickness of the water layer $\tilde{\tau}_w$ is equal to $\kappa_w|h_w|$.

According to Eq. (8) and boundary condition (6), the diffuse radiance $I^{\uparrow}(\tilde{\tau}_w)$ is decreased by a factor $\exp\!\left(-\dfrac{\tilde{\tau}_w}{\eta}\right)$ along the direction (η, ϕ) between the pond bottom and top of the water layer. It is then reduced by a factor $R(\eta)$ at the air-water interface and, finally, by another factor $\exp\!\left(-\dfrac{\tilde{\tau}_w}{\eta}\right)$ along the direction $(-\eta, \phi)$ before reaching the pond bottom again.

Inserting $I^{\uparrow}(\tilde{\tau}_w)R(\eta')\exp\!\left(-\dfrac{2\tilde{\tau}_w}{\eta'}\right)$ into the right side of Eq. (10) and integrating over η', the solution to Eq. (8) is written as follows

$$I^{\uparrow}\,(\tilde{\tau}, \eta) = \frac{\alpha_i(1 - R(\mu_0))F_0 \exp\!\left(-\dfrac{\tilde{\tau}_w}{\eta_0} - \dfrac{\tilde{\tau}_w - \tilde{\tau}}{\eta}\right)}{\pi(1 - 2\alpha_i R_3(2\tilde{\tau}_w))}, \tag{11}$$

and

$$I^{\downarrow}\,(\tilde{\tau}, -\eta)$$
$$= \frac{\alpha_i R(\eta)(1 - R(\mu_0))F_0 \exp\!\left(-\dfrac{\tilde{\tau}_w}{\eta_0} - \dfrac{\tilde{\tau}_w + \tilde{\tau}}{\eta}\right)}{\pi(1 - 2\alpha_i R_3(2\tilde{\tau}_w))}, \tag{12}$$

where

$$R_3(t) = \int_0^1 R(\eta)\exp\!\left(-\frac{t}{\eta}\right)\eta\,d\eta, \tag{13}$$

is a generalisation for the third exponential integral (Abramowitz & Stegun 1964)

$$E_3(t) = \int_0^1 \exp\!\left(-\frac{t}{\eta}\right)\eta\,d\eta. \tag{14}$$

Integrating $(1 - R(\eta))I^{\uparrow}(0, \eta)\eta$ over the upper hemisphere yields $F^{\uparrow}(0)$, the upwelling irradiance just above the air-water interface. Dividing $F^{\uparrow}(0)$ derived from Eq. (11) by F_0 and adding the Fresnel reflection coefficient for the air-water interface, we obtain an expression for α_w, the spectral albedo for the melt pond of optical thickness $\tilde{\tau}_w$ under direct illumination for the case of a

Lambertian bottom:

$$\alpha_w(\tilde{\tau}_w) = R(\mu_0)$$

$$+ \frac{2\alpha_i(1 - R(\mu_0))(E_3(\tilde{\tau}_w) - R_3(\tilde{\tau}_w))\exp\left(-\dfrac{\tilde{\tau}_w}{\eta_0}\right)}{1 - 2\alpha_i R_3(2\tilde{\tau}_w)}$$

$$(15)$$

As earlier, μ_0 and η_0 are related by Eq. (1).

Parameterisation of the function $R_3(t)$

The goal of this section is to parameterise the function $R_3(t)$ so that α_w can be computed efficiently. Because melt ponds are unlikely to be deeper than 1 m in the Arctic, actual values of $\tilde{\tau}_w$ are unlikely to exceed 1 in the visible spectrum according to data on κ_w compiled by Smith & Baker (1981). Consequently, the following series expansion can be used for calculating $E_3(t)$:

$$E_3(t) = \frac{t^2}{2}\left(-\ln(t) - C + \frac{3}{2}\right) - \sum_{\substack{m=0 \\ m \neq 2}}^{\infty} \frac{(-1)^m t^m}{(m-2)m!},$$

$$(16)$$

where C is the Euler constant. A convenient expression for $R_3(t)$ is easily derived from Eq. (13)

$$R_3(t) = E_3(t) - \int_{\eta_{cr}}^{1} (1 - R(\eta))\exp\left(-\frac{t}{\eta}\right)\eta d\eta,$$

$$(17)$$

where

$$\eta_{cr} = \frac{\sqrt{n_w^2 - 1}}{n_w}$$

$$(18)$$

denotes the cosine of the critical angle for total internal reflection. Expanding $\exp\left(-\dfrac{t}{\eta}\right)$ in a power series, we get

$$E_3(t) - R_3(t) = \sum_{m=0}^{\infty} (-1)^m r_m t^m,$$

$$(19)$$

where r_m is given by

$$r_m = \frac{1}{m!}\int_{\eta_{cr}}^{1} (1 - R(\eta))\eta^{1-m}d\eta.$$

$$(20)$$

When Eqs. (16) and (19) are employed to calculate $E_3(t)$ or $E_3(t) - R_3(t)$, the summation over index m is performed from 0 to a finite number M.

Finally, let us evaluate $R_3(0)$ which is a prerequisite for calculating radiometric quantities for an optically thin melt pond. It is seen from Eq. (14) that $E_3(0) = 0.5$. According to Eq. (13), $2R_3(0)$ is equal to the internal reflectance of radiation at the air-water interface for radiation incident from below r_+, for the case of a uniform radiance distribution at a plane water surface (Preisendorfer 1976). The r_+ values are in the range from 0.47 to 0.49 for the visible spectrum (Preisendorfer 1976). Consequently, the value of $R_3(0)$ is about half the value of $E_3(0)$.

Monte Carlo simulations

Monte Carlo method was employed to find an "exact" solution to Eq. (2) with the boundary conditions given by Eqs. (6) and (7). Comparison of the Monte Carlo solution to Eq. (2) and the analytical solution to Eq. (8) enables us to estimate errors of the analytical solution. These errors arise due to scattering of radiation in the water layer. The estimated errors give a measure of the precision of Eq. (15) in calculating the pond albedo over the wavelength region of interest.

The method to be applied in Monte Carlo simulations is similar to the methods reported earlier in the context of computing underwater light fields (see Mobley 1994 for references). In particular, a weight W_0 is assigned to each photon as follows

$$W_0 = \exp(-\kappa_w \zeta_w) \prod_{k=1}^{K} R(\eta_k).$$

$$(21)$$

Here ζ_w is the path length of the photon, K is the number of Fresnel reflections from the water-air interface, and $R(\eta_k)$ is the Fresnel reflection coefficient for radiation incident from below the interface. Two detectors are used: the first to determine the upwelling irradiance $F^\uparrow(0)$ just above the water surface, and the second to determine the downwelling irradiance $F^\downarrow(\tau_w)$ just above the pond bottom. The one-dimensional (the coordinate τ) path of each photon is followed until the photon strikes the bottom twice. The coordinate η is used explicitly to determine the direction of the photon travel. In turn, the coordinate ϕ is employed implicitly to compute a new value of η in accordance with Eqs. (3) and (4) when a scattering interaction takes place.

Gordon & Brown (1974) introduced a modification of the Monte Carlo method to assess the influence of bottom albedo on the diffuse

reflectance of a plane-parallel ocean as a function of bottom depth and albedo. As this problem is very close to that addressed here, the method of Gordon & Brown (1974) is applicable to our study. In particular, an expression for the upwelling irradiance measured by the first detector (above the water surface) is written as

$$F^{\uparrow}(0) = F_0^{\uparrow}(0) + \frac{\alpha_i F_1^{\uparrow}(0)}{1 - \alpha_i \rho}, \tag{22}$$

where $F_0^{\uparrow}(0)$ is the contribution to $F^{\uparrow}(0)$ from photons that do not strike the bottom, $F_1^{\uparrow}(0)$ is the contribution to $F^{\uparrow}(0)$ from photons that strike the bottom once for $\alpha_i = 1$, and ρ is the ratio of the contribution to $F^{\downarrow}(\tau_w)$ from photons that strike the bottom twice to the contribution from photons striking the bottom once for $\alpha_i = 1$. So, the value $\alpha_i = 1$ is applied to both contributions which form the ratio ρ, but the actual value of α_i is then used to determine $F^{\uparrow}(0)$ from Eq. (22). The important thing to mention is that the factor $(1 - \alpha_i\rho)^{-1}$ in Eq. (22) accounts for all the multiple reflections.

The computations were carried out for the case of Rayleigh scattering. Accordingly, the phase function was specified by

$$x(\gamma) = \frac{3}{4}(1 + \cos^2(\gamma)). \tag{23}$$

Although the Λ_w values for the clearest water do not exceed 0.31 in the 400–700 nm wavelength region (Smith & Baker 1981), our calculations were made for an overestimated value of $\Lambda_w = 0.5$. Moreover, the maximum possible value for the spectral albedo of melting white ice, $\alpha_i = 0.8$ (Grenfell & Maykut 1977), was used. Thus, the effect of scattering on the pond albedo may be slightly overestimated. The maximum relative statistical error in estimating α_w by the Monte Carlo method was about 1.5%.

Shown in Fig. 2 are the α_w values versus τ_w calculated for a solar zenith angle of 60°. Curve I (dashed line) represents the "exact" Monte Carlo solution. Curves II and III represent albedos calculated for the non-scattering water layer, i.e. either directly from Eq. (15) (solid line) or using parameterisations (16) and (19) with M = 4 (dotted line). τ_w is determined from $\tilde{\tau}_w$ using Eq. (9). As seen from Fig. 2, scattering has no effect on α_w whenever $\tau_w < 1$. Beyond the visible spectrum τ_w can exceed 1 for actual ponds, but Λ_w is negligible for wavelengths exceeding 700 nm. Eq.
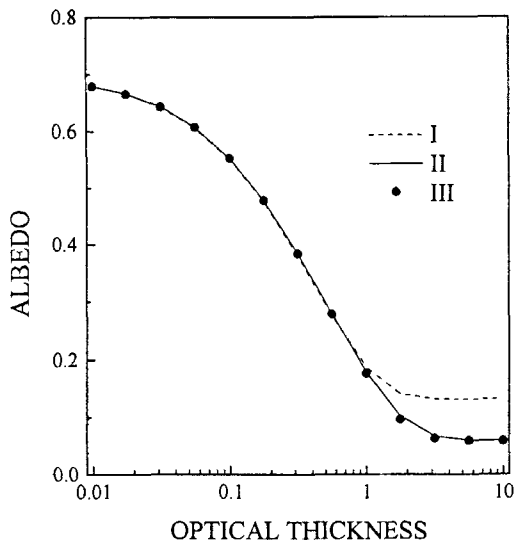

Fig. 2. Melt-pond albedo versus optical thickness of the water layer calculated using (I) the Monte Carlo method, (II) analytical expression (15), and (III) calculations using analytical expression (15) where functions $E_3(t)$ and $R_3(t)$ are computed using expressions (16) and (19).

(15) and, thus, parameterisations (16) and (19) (M = 4) are used below to compute α_w.

Observations

Measurements in the Barents Sea

The observational data presented in this study were collected during the R/V LANCE cruise in the northern part of the Barents Sea in August 1993 under the Russian-Norwegian Oceanographic Programme (RUSNOP). Measurements of pond albedo were carried out on 12 August 1993 over a small multiyear floe with a diameter of about 150 m located near 78.8°N, 34.8°E. Measurements were also made of the albedo of the melting bare ice. The ice thickness was approximately 2 m. Glitter patterns on the pond surfaces were not observed. Wind speed was about 2 m/s.

A quantum sensor LI-190 SB with a spectral window of 400–700 nm was employed to measure both the incident and reflected irradiances over a sequence of melt ponds of varying depths. The sensor was located about 0.2 m above the water surface and between 1.5 and 2.0 m away from the bare ice to avoid reflected radiance from outside the melt pond surface.

All albedo measurements were made under clear skies at about 1200 solar time. The solar zenith angle was about 60° and the full solar disc was visible. Weather and illumination conditions were stable during the observations. Measurements of upwelling and downwelling irradiances for each individual pond were made between three and five times in order to estimate mean values and standard deviations of albedo. Moreover, before measurements were made, every melt pond was tested visually for the presence of bottom contamination, and only uncontaminated, clean ponds were selected. No clean ponds were found with a depth exceeding 0.35 m; one reference measurement was made for a comparatively deep (0.5 m) contaminated pond.

As seen from Table 1, the measured albedo at $h_w = 0.5$ m is as low as 0.35 compared to 0.59 observed at $h_w = 0.35$ m. This is clearly connected, in our opinion, with cryoconite holes (Eicken et al. 1994) that were observed on the bottom of the deepest pond. According to Eicken et al. (1994), the occurrence of cryoconite holes is a consequence of contaminants deposited on the pond bottom and is linked, therefore, to a decreased value of pond albedo. At the same time, the albedos reported in Table 1 for the shallow ($h_w < 0.35$ m) ponds are nearly independent of pond depth.

Comparison with other data sets

These albedos are in reasonable agreement with observations made by other investigators. In particular, Ivanov & Alexandrov (1994) carried out measurements north of Franz Josef Land during an expedition aboard R/V POLARSTERN in August 1993 and found spectrally-averaged albedos of clean ponds to be 0.30 ± 0.05 for depths less than 0.3 m, and 0.26 ± 0.03 for depths in the range of 0.30 to 0.50 m. Although these albedo values are lower than those shown in Table 1 for the shallow ponds, the difference can be partly attributed to employing the model PP-1 pyranometer which has a spectral window of 390–780 nm, for the measurements performed by Ivanov & Alexandrov (1994).

Morassutti & LeDrew (1995) calculated regression curves for pond albedo in the 400–700 nm wavelength band versus pond depth based on an analysis of several hundred field measurements. The regression curve, reported for the case of clear sky, demonstrates a sharp decrease in a depth range from 0 to 0.1 m but is almost constant at larger depths.

Spectrally-averaged albedo of melt ponds

We used a simplified approach to compute the incident irradiance reaching the surface. Because the atmosphere was assumed to be cloudless and aerosol-free, only the absorption of solar radiation by O_3 was taken into account. Absorption by water vapor and other gases was ignored because their effect on solar radiation is insignificant over the spectral region of interest (e.g. Liou 1992). Furthermore, Rayleigh scattering in the atmosphere was also ignored. First, the direct incident irradiance reaching the surface exceeds the downwelling diffuse irradiance by an order of magnitude for the solar zenith angle of 60°. Second, the Fresnel external reflectance for the case of uniform radiance at a plane water surface is about 0.066 (Preisendorfer 1976) and is close to the observed value of $R(\mu_0)$ of about 0.060 for $\theta_0 = 60°$.

Table 1. Albedo of melt ponds in the 400–700 nm wavelength band versus pond depth.

Pond depth (m)	Melt pond bottom (top surface of the bare ice)	Albedo	Standard deviation
bare ice	clean	0.84	0.05
0.02	clean	0.54	0.02
0.10	clean	0.53	0.01
0.19	clean	0.56	0.02
0.35	clean	0.59	0.02
0.50	contaminated	0.35	0.02

The measurements of spectral albedo reported by Grenfell & Maykut (1977) for melting multiyear white ice were used to specify α_i. Absorption of solar radiation by O_3 in the Chappuis band for the total ozone content equivalent to 0.5 cm was calculated according to Nicolet (1981). The κ_w values were taken from Smith & Baker (1981).

Spectrally averaged broadband albedo, $\langle \alpha_w \rangle$, for a spectral region (λ_1, λ_2) is introduced as follows

$$\langle \alpha_w \rangle = \frac{\int_{\lambda_1}^{\lambda_2} \alpha_w(\bar{\tau}_w(\lambda)) F_0(\lambda) d\lambda}{\int_{\lambda_1}^{\lambda_2} F_0(\lambda) d\lambda}, \quad (24)$$

where $F_0(\lambda)$ is the distribution of the incident spectral irradiance.

The integration was performed from $\lambda_1 = 400$ nm to $\lambda_2 = 700$ nm with a step of 10 nm. $\theta_0 = 60°$ was used. The zero value of h_w corresponds to both bare ice and ponds of infinitesimally small depth, hereafter referred to as "newly formed" melt ponds. The calculated $\langle \alpha_w \rangle$ are plotted in Fig. 3 together with the measurements reported in Table 1.

Discussion

Although the differences between calculated and observed albedos are significant, two conclusions can still be drawn from Fig. 3. The first conclusion is that a step-decrease in albedo is likely to occur when a melt pond forms. In order to address this issue in more detail, we write Eq. (15) for $\bar{\tau}_w = 0$. Clearly, this is the case of the newly formed melt pond. Taking into account that $2R_3(0) = r_+$ for the case of a Lambertian bottom, we obtain from Eq. (15)

$$\alpha_w(0) = R(\mu_0) + \frac{\alpha_i(1 - R(\mu_0))(1 - r_+)}{1 - \alpha_i r_+}. \quad (25)$$

Eq. (25) allows us to determine $\Delta \alpha_i$, the difference between $\alpha_w(0)$ and α_i,

$$\Delta \alpha_i = \alpha_w(0) - \alpha_i = -\frac{(\alpha_i r_+ - R(\mu_0))(1 - \alpha_i)}{1 - \alpha_i r_+}. \quad (26)$$
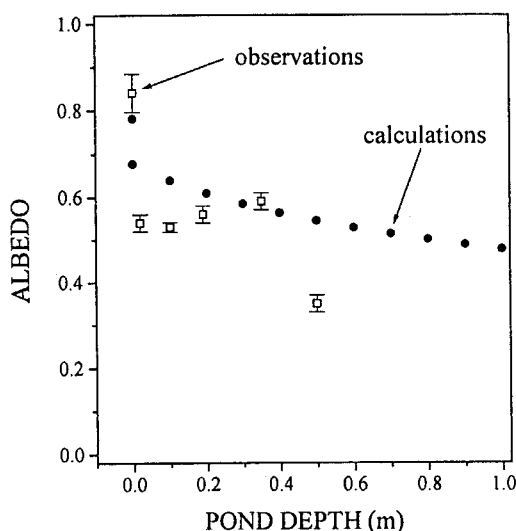

Fig. 3. Measured and calculated albedos for melt ponds and bare ice in the 400–700 nm wavelength band. Vertical bars represent standard deviations.

As seen from Eq. (26), $\Delta \alpha_i$ is negative if $\alpha_i r_+ > R(\mu_0)$. This is satisfied for actual values of α_i and θ_0. The maximum absolute value of $\Delta \alpha_i$ is about 0.12 for $\alpha_i = 0.6$ and $\theta_0 = 60°$.

According to Mullen & Warren (1988), who calculated the spectral albedo of lake ice, the external surface reflectance tends to increase albedo over what it would be without the surface layer (air-ice interface, in our case), whereas internal reflection directs radiation back down tending to decrease albedo. With respect to the problem addressed in this paper, one may conclude that the spectral albedo of the ice layer beneath the pond is larger than the spectral albedo of the bare ice with the same optical properties under conditions where the solar zenith angle is not too large.

On the other hand, an analysis of Table 1 of this study and fig. B8a from Morassutti & LeDrew (1995) suggests that there exists a difference between the albedos of newly formed pond and bare ice; the magnitude of this difference is about 0.1–0.3 in the 400–700 nm wavelength band. Moreover, a similar sharp decrease in spectral albedo was reported by Perovich (1994) for a shallow (0.03 m) melt pond. Finally, this difference is also observed in our calculations of melt pond albedo reported in Fig. 3. Thus, the only way to explain both observed and modelled

step-decreases in albedo is to postulate that the changes in structural and optical properties of the bottom, which occur when the melt pond forms, cause a greater decrease than predicted by Eq. (26).

To assess the influence of the assumption that the melt pond bottom is a Lambertian reflector, the case where this assumption is relaxed is examined. A convenient way to parameterise the upwelling radiance for the newly formed pond is to use the cardioidal radiance distribution

$$I^\uparrow(0, \eta) = I^\uparrow(0,0)(1 + \varepsilon\eta), \qquad (27)$$

where ε is a parameter. Lambertian reflectance is the special case of $\varepsilon = 0$. Under the assumption that the law of diffuse reflectance for the pond bottom is independent of the direction of the incident radiation, Eq. (25) is still valid for the radiance distribution given by Eq. (27). This can be shown by applying Eq. (22) to the newly formed pond. When $\alpha_i = 1$ and absorption of the radiation in the water layer is negligible, the average contribution to the upwelling radiance just above the air-water interface from photons that do not strike the bottom is exactly $R(\mu_0)$, while the contribution from photons striking the bottom once is $(1 - R(\mu_0))(1 - r_+)$. Furthermore, the ratio of the contribution to the downwelling irradiance at the pond bottom from photons that strike the bottom twice to the contribution from photons striking the bottom once is r_+ for the case of $\alpha_i = 1$. Incorporating $\rho = r_r$ and the above considerations into Eq. (22) yields Eq. (25).

In accordance with Eq. (27), r_+ calculated for negative (positive) ε is larger (smaller) than r_+ calculated for the case of a Lambertian bottom. When $\varepsilon > 0$, radiation is redirected into a more nearly normal direction and it is easier, therefore, for it to escape from the melt pond due to the reduced Fresnel reflection at the small zenith angles. Alternatively, for $\varepsilon < 0$, radiation is more likely to be reflected back to the bottom. Thus, deviations from Lambertian behaviour can cause either an increase or reduction of $\Delta\alpha_i$. A negative ε has a stronger effect on the absolute value of $\Delta\alpha_i$. For example, when $\varepsilon = -0.9$ (which is representative for the upwelling radiance distribution observed in the upper ocean), and $\alpha_i = 0.8$, $\alpha_w(0) = 0.57$ because r_+ would be about 0.7 (Preisendorfer & Mobley 1985). The reference value of $\alpha_w(0)$ for $\varepsilon = 0$ is as large as 0.7

As mentioned above, wind speeds during our observations were too small (2 m/s) to produce capillary wave slopes sufficient to cause a significant effect on the penetration of radiation into the melt pond. The effect of capillary waves can be stronger, however, when a high wind speed is combined with a comparatively large (>60°) solar zenith angle. The major contribution to the albedo change in this case would be due to the reduced Fresnel reflection of the incident radiation, whereas the effect of capillary waves on the internal reflection would be smaller according to Preisendorfer & Mobley (1985). Therefore, with respect to the melt pond albedo, possible deviations from Lambertan behavior of the pond bottom seem to be more important than the effect of capillary waves.

The step-decrease in albedo is associated with a variation in $F^\downarrow(\tilde{\tau}_w)$, the downwelling irradiance entering the ice layer. For the case of direct illumination, contribution to $F^\downarrow(\tilde{\tau}_w)$ from the diffuse radiation field can be found by integrating $I^\downarrow(\tilde{\tau}_w, -\eta)\eta$ (see Eq. (12)) over the lower hemisphere. The contribution from the direct radiation field is $F^\downarrow_{dir}(\tilde{\tau}_w)$ (see Eq. (5)). As a result, we have

$$F^\downarrow(\tilde{\tau}_w) = T_w(\tilde{\tau}_w)F_0 \qquad (28)$$

where

$$T_w(\tilde{\tau}_w) = \frac{(1 - R(\mu_0))\exp\left(-\dfrac{\tilde{\tau}_w}{\eta_0}\right)}{1 - 2\alpha_i R_3(2\tilde{\tau}_w)} \qquad (29)$$

denotes spectral transmissivity of the water layer. It can be shown using Eqs. (15) and (29) that spectral albedo of the newly formed pond and its spectral transmissivity are related by the expression

$$T_w(0) = \frac{1 - \alpha_w(0)}{1 - \alpha_i}. \qquad (30)$$

Thus, $T_w(0) > 1$ if $\Delta\alpha_i < 0$.

The second conclusion from Fig. 3 is that the melt pond albedo depends more on the optical properties of the bottom than on pond depth. To evaluate the effect of absorption of the shortwave radiation in the water on pond albedo, let us determine the spectral radiative energy flux into the water layer (H_w). The upwelling irradiance at the ice-water interface can be found

Table 2. Spectral albedo of a melt pond, spectral transmissivity of the water layer and spectral radiative energy fluxes into the water and ice layers at $\lambda = 500$ nm as functions of pond depth ($\alpha_i = 0.8$).

Pond depth (m)	α_w	T_w	H_w/F_0	H_i/F_0
0.0	0.70	1.51	0	0.30
0.1	0.69	1.49	0.01	0.30
1.0	0.62	1.36	0.11	0.27

by multiplying Eq. (28) by α_i:

$$F^\uparrow(\bar{\tau}_w) = \alpha_i T_w(\bar{\tau}_w) F_0. \qquad (31)$$

The difference between $F^\downarrow(\bar{\tau}_w)$ and $F^\uparrow(\bar{\tau}_w)$ is the special radiative energy flux into the ice layer:

$$H_i = (1 - \alpha_i) T_w(\bar{\tau}_w) F_0. \qquad (32)$$

Finally, H_w can be obtained by subtracting H_i from $(1 - \alpha_w) F_0$:

$$H_w = \big(1 - \alpha_w - (1 - \alpha_i) T_w(\bar{\tau}_w)\big) F_0. \qquad (33)$$

Table 2 shows the spectral melt pond albedos, spectral transmissivities of the water layer and spectral radiative energy fluxes into the ice and water layers computed for three different values of h_w using Eqs. (15), (29), (32) and (33). These values represent a newly formed pond, a shallow pond and a deep pond respectively. Calculations are performed for $\lambda = 500$ nm and $\alpha_i = 0.8$. For convenience, the radiative fluxes are presented relative to F_0 so that knowledge of the absolute value of F_0 is unnecessary.

The results reported in Table 2 enable us to evaluate the effect of absorption of short-wave radiation in the water layer on the melt pond albedo. The effect is negligible for shallow ponds, and should be taken into account only for deep ponds. Nevertheless, the usually observed difference between spectral albedos of melting bare ice (as high as 0.8 at $\lambda = 500$ nm for the white ice) and deep ponds (as low as 0.2–0.3 at $\lambda = 500$ nm for the old ponds) (e.g. Grenfell & Maykut 1977) is unlikely to be explained only by absorption of the radiation in the water layer which is rather transparent to the radiation in the visible spectrum. The major contribution to this difference should be attributed to the optical and structural properties of the underlying ice.

Conclusions

In this study, we have both empirically and theoretically examined melt pond albedos in the 400–700 nm wavelength band as a function of the pond depth. An analytical approximation of spectral albedo was derived for a pond with a Lambertian bottom, assuming that Rayleigh scattering in the water is small compared to absorption. Using a Monte Carlo method, it was shown that scattering in the water can be ignored.

Measurements of albedo in clean ponds were made in the Barents Sea in August 1993 under clear sky conditions. Comparison of observations and theoretical calculations indicates that (1) a step-decrease in albedo is likely to occur when a melt pond initially forms, and (2) melt pond albedos depend more on the structural and optical properties of the underlying ice than on pond depth. The effect of absorption of short-wave radiation in the water on melt pond albedos needs to be taken into account for the deep ponds only.

The analytical approximation to the melt pond spectral albedo can be inverted and applied to estimating the spectral albedo of melt pond bottoms as described by Podgorny (1995). This enables us to determine the redistribution of solar energy between the melt pond and underlying ice from measurements of pond albedo and depth using the forward model developed in this paper.

References

Abramowitz, M. & Stegun, I. A. (Eds.) 1964: Handbook of mathematical functions with formulas, graphs and mathematical tables. National Bureau of Standards, Applied Mathematics Series – 55.

Barry, R. G., Serreze, M. C., Maslanik, J. A. & Preller, R. H. 1993: The Arctic sea ice-climate system: observations and modelling. *Rev. Geophys. 31*, 397–422.

Ebert, E. E. & Curry, J. A. 1993: An intermediate one-dimensional thermodynamic sea ice model for investigation ice

atmosphere interactions. *J. Geophys. Res. 98 (C6)*, 10085–10109.

Ebert, E. E., Schramm, J. L. & Curry, J. A. 1995: Disposition of solar radiation in sea ice and the upper ocean. *J. Geophys. Res. 100 (C8)*, 15965–15975.

Eicken, H., Alexandrov, V., Gradinger, R., Ilyin, G., Ivanov, B., Luchetta, A., Martin, T., Olsson, K., Reimnitz, E., Pac, R., Poniz, P. & Weissenberger, J. 1994: Distribution, structure and hydrography of surface melt puddles. *Ber.Polarforsch. 149*, 73–76.

Gordon, H. R. & Brown, O. B. 1974: Influence of bottom depth and albedo on the diffuse reflectance of a flat homogeneous ocean. *Appl. Opt. 13(9)*, 2153–2159.

Grenfell, T. C. & Maykut, G. A. 1977: The optical properties of ice and snow in the Arctic basin. *J. Glaciol. 18(80)*, 445–463.

Grenfell, T. C. & Perovich, D. K. 1984: Spectral albedos of sea ice and incident solar irradiance in the Southern Beaufort Sea. *J. Geophys. Res. 89 (C3)*, 3573–3580.

Ivanov, B. V. & Alexandrov, V. 1994: Albedo of the ice cover during late summer time and energy exchange process. *Ber. Polarforsch. 149*, 47–51.

Jin, Z., Stamnes, K., Weeks, W. F. & Tsay, S. C. 1994: The effect of sea ice on the solar energy budget in the atmosphere-sea ice-ocean system: a model study. *J. Geophys. Res. 99(C12)*, 25281–25294.

Langleben, M. P. 1971: Albedo of melting sea ice in the Southern Beaufort sea. *J. Glaciol. 10 (58)*, 101–104.

Liou, K. N. 1992: *Radiation and cloud processes in the atmosphere*. Oxford University Press. 487 pp.

Maykut, G. A. 1986: The surface heat and mass balance. Pp. 395–463 in Untersteiner N. (ed.): *The geophysics of sea ice*. Martinus Nijhoff Publ., Dordrecht (NATO ASI B146).

Maykut , G. A. & Perovich, D. K. 1987: The role of short-wave radiation in the summer decay of a sea ice cover. *J. Geophys. Res. 92 (C7)*, 7032–7044.

Mobley, C. D. 1994: *Light and water. Radiative transfer in natural waters*. Academic Press Inc. 592 pp.

Morassutti, M. P. & LeDrew, E. F. 1995: Melt pond dataset for use in sea-ice and climate-related studies. ISTS-EOL-TR95-001, Earth-Observations Lab., ISTS and Dept. Geog., University of Waterloo, Ontario, Canada. 53 pp.

Moritz, R. E., Curry, J. A., Thorndike, A. S. & Untersteiner, N. (Eds.) 1993: SHEBA. A Research Program on the Surface Heat Budget of the Arctic Ocean. APL-UW, Seattle. 33 pp.

Mullen, P. C. & Warren, S. G. 1988: Theory of optical properties of lake ice. *J. Geophys. Res. 93 (D7)*, 8403–8414.

Nazincev, Ju. L. 1964: Teplovoj balans poverchnosti morskogo ledjanogo pokrova v Central'noj Arktike (Heat balance of the surface of the multiyear ice cover in the Central Arctic). *AANII, Trudy*, 267, 110–126.

Nicolet, M. 1981: The solar spectral irradiance and its action in the atmospheric photodissociation processes. *Planet. Space Sci. 29 (9)*, 951–974.

Perovich, D. K. 1994: Light reflection from sea ice during the onset of melt. *J. Geophys. Res. 99 (C2)*, 3351–3359.

Podgorny, I. A. 1995: Measurement of the optical characteristics of a puddle. *Russian Meteorology and Hydrology, N3*, 50–58.

Preisendorfer, R. W. 1976: Hydrologic optics. Vol. 6: Surfaces. Pacific Marine Environmental Laboratory, ERL-NOAA, Seattle. 390 pp.

Preisendorfer, R. W. & Mobley, C. D. 1985: Unpolarized irradiance reflectances and glitter patterns of random capillary waves on lakes and seas, by Monte Carlo simulation. NOAA Tech. Memo. ERL PMEL-63, Pacific Marine Environmental Laboratory, ERL-NOAA, Seattle. 141 pp.

Smith, R. C. 1973: Optical properties of the Arctic upper water. *Arctic 26 (4)*, 303–313.

Smith, R. C. & Baker, K. S. 1981: Optical properties of the clearest natural waters (200–800 nm). *Appl. Opt. 20 (2)*, 177–184.

Notation

E_3	the third exponential integral
F_0	incident spectral irradiance (W m^{-2} nm^{-1})
$F^{\downarrow}$	downwelling spectral irradiance (W m^{-2} nm^{-1})
$F^{\uparrow}$	upwelling spectral irradiance (W m^{-2} nm^{-1})
h_w	thickness of the water layer or pond depth (m)
H_i	spectral radiative energy flux into the ice layer (W m^{-2} nm^{-1})
H_w	spectral radiative energy flux into the water layer (W m^{-2} nm^{-1})
I	diffuse spectral radiance (W m^{-2} nm^{-1} sterad^{-1})
$I^{\downarrow}$	diffuse downwelling radiance (W m^{-2} nm^{-1} sterad^{-1})
$I^{\uparrow}$	diffuse upwelling radiance (W m^{-2} nm^{-1} sterad^{-1})
n_w	refractive index of the water
r_+	internal reflectance of the air-water for uniform illumination
$R(\mu_0)$	Fresnel reflection coefficient for irradiance incident on the air-water from above
$R(\eta)$	Fresnel reflection coefficient for irradiance incident on the air-water from below
R_3	Fresnel reflection integral
T_w	spectral transmissivity of the water layer for the downwelling irradiance
W_0	weight assigned to a photon
$\times$	phase function
α_i	spectral albedo of the ice layer, $(F^{\uparrow}(\tau_w)/F^{\downarrow}(\tau_w)$
α_w	spectral albedo of the melt pond
$\alpha_w(0)$	spectral albedo of the newly formed pond
$\langle \alpha_w \rangle$	spectrally averaged albedo of the melt pond
γ	scattering angle
ε	parameter of the cardioidal radiance distribution
$\Delta\alpha_i$	difference between $\alpha_w(0)$ and α_i
ζ_w	path length of photon in the water layer
η	cosine of zenith angle in the water layer
η_0	cosine of zenith angle for direct solar radiation in the water layer
η_{cr}	cosine of the critical angle for total internal reflection
θ_0	solar zenith angle (degrees)
κ_w	spectral absorption coefficient of the water (m^{-1})
λ	wavelength (nm)
Λ_w	single-scattering albedo of the water
μ	cosine of zenith angle in the atmosphere
μ_0	cosine of the solar zenith angle
σ_w	scattering coefficient of the water (m^{-1})
τ	optical depth
τ_w	optical thickness of the water layer (exact solution)
$\tilde{\tau}_w$	optical thickness of the water layer (analytical solution)
ϕ	azimuthal angle (degrees)
ϕ_0	solar azimuthal angle (degrees)